Mathematical Simulation of Dynamic Coupled Heat and Liquid Moisture Transfer in Multilayer Anisotropic Porous Polymers

Y. Li, Z. Wang

Institute of Textiles and Clothing, The Hong Kong Polytechnic University, Hung Hum, Kowloon, Hong Kong, China

Received 8 December 2003; accepted 26 April 2004
DOI 10.1002/app.20916
Published online in Wiley InterScience (www.interscience.wiley.com).

ABSTRACT: A one-dimensional mathematical model describing the dynamic coupled heat and moisture transfer inside multilayered porous polymers and anistropic materials is developed in this reported study. Compared to models published previously, three improvements have been made: (1) the model takes into account the dynamic complex behavior of coupled heat and liquid moisture transfer inside each layer; (2) the model provides different (inter-) boundary conditions that correspond with the contact situations between neighbored layers and the influences from waterproof fabrics; and (3) the combinations of different types of polymer fibers in each layer and their roles with respect to processes of heat and moisture transfer. Physical experiments for liquid transfer, through the layered fabric assemblies with different construction, were carried out to validate the developed model in terms of dynamic temperature and moisture concentration distribution in the assembly, as well as the initial and final absolute liquid volumetric fractions at the surface of the top layer. Good agreement between the calculated and experimental results was obtained. © 2004 Wiley Periodicals, Inc. J Appl Polym Sci 94: 1590–1605, 2004

Key words: fibers; computer modeling; simulations; heat and moisture transfer; heterogeneous polymers

INTRODUCTION

A clothing system and the confined air layer between skin and the inner clothing surface, as well as between the clothing layers, act as serially connected resistances to heat and moisture flow. This provides the theoretical foundation for Farnworth's and Lotens's numerical model of the combined diffusion of heat and water vapor through layered clothing.[1–4] Farnworth assumed the uniform phase of water presence in each layer; therefore, in each layer, condensation and absorption cannot coexist. The thermal resistance R_{Hi} was expressed by a combination of air thermal conductivity and an effective radiative component. The vapor resistance R_{Vi} was assigned a different value for different cases. Both R_{Hi} and R_{Vi} are dependent on the thickness and the weave density of the fabric.[1] In the models proposed by Lotens et al.,[2–4] two parallel resistance chains, including the resistances to heat flow and moisture flows, exist in the system, and the two chains are correlated with the phase change processes such as moisture vapor condensation and absorption at the layer conjunction. Radiant heat transfer was also considered.

Gibson and Charmchi[5] reported a theoretical mathematical model for the coupled heat and moisture transfer through porous polymer materials by using a volume-averaging technique to derive numerical solutions. The model was also applied to study the interactions between human thermoregulation and the clothing layers.[6] They also applied the simplified one-dimensional form of equations to predict the behavior of transient diffusion of coupled heat and moisture flow through groups of porous materials made of different textile fibers and obtained good agreement with experimental temperature profiles of the materials.

These models have similar features:

1. They consider a layer of fabric or clothing as isotropic in terms of thermal and moisture status and transport status. These assumptions allow the models to be described as simple linear mathematical forms, which can be solved more easily.
2. Although different processes of heat and moisture transfer were considered, together with the coupled mechanisms, the isotropic assumption limits the ability of the models to describe the dynamic thermal and moisture transfer pro-

Correspondence to: Y. Li (tcliyi@inet.polyu.edu.hk).
Contract grant sponsor: Hong Kong Grant Research Committee.
Contract grant sponsor: Hong Kong Polytechnic University; contract grant numbers: PolyU5111/98E, PolyU5151/01E, A188.

cesses inside a single layer of fabric, particularly in textile fibers.
3. These models did not consider the liquid transfer mechanisms in the system.

Because of these limitations, the models published previously cannot be used to solve some complex problems, in which multilayer textile materials are used to absorb and remove liquid water from the skin surface. For instance, multilayer textile materials are used to make diapers and bedding materials for taking care of infants and incontinent patients. Therefore, this article proposes a new mathematical model for multilayer anisotropic porous polymer materials based on the published model for isotropic structures.[7] New developments have been made in the following areas:

1. The complex mechanisms of dynamic coupled heat and moisture transfer in every layer of the layered assembly are considered, including the liquid transfer.
2. New boundary conditions are developed for every layer in terms of contact situation and waterproof fabric presence at both inner and outer surfaces.
3. The influences from different types of polymer fibers on the heat and moisture transfer processes are considered. Those effects are combined linearly in terms of the volumetric fractions of different types of fiber.

A series of experiments, which simulate the infant bed-wetting process, were also carried out to validate the new model and comparisons between calculated and measured results are discussed.

PHYSICAL MECHANISMS AND MATHEMATICAL FORMULATION

Physical mechanisms

The mechanisms of the multiphase-coupled heat and moisture transfer in a multilayer anisotropic porous material model are similar to those involved in the isotropic porous material.[7] Heat is transferred by conduction and radiation, and is generated through the moisture-phase changes such as moisture sorption and condensation/evaporation inside the fabrics. Moisture is transferred by diffusion through the void space inside and through the fiber, liquid water transfer between the fibers, and is also affected by the phase change process mentioned above. In addition, the nature of heat and moisture transfer in multilayers and anisotropic materials requires consideration of two issues: (1) the roles played by different materials in each layer; (2) the mechanisms of heat and moisture (vapor and liquid) exchange at the interfaces between neighboring layers.

Model development

System description

A schematic diagram for an n-layer fabric assembly ($n \geq 2$) with different configurations of fiber types in each layer is illustrated in Figure 1. The governing mechanisms for the coupled heat and moisture transfer inside each layer are the same as those in the model of isotropic materials, reported in Wang et al.,[7] are thus omitted here.

A multilayer anisotropic porous polymer material, such as a textile assembly, is constructed in terms of geometrical features, layer relationship, fiber type composition, and the combined physical properties of different fiber types, which is explained as follows:

1. All fabric layers (L_1, L_2, ..., L_n) are serially interfaced.
2. I_{i0} and I_{i1} are defined to represent the thickness of the left gap and right gap, respectively, between neighboring layers; I_{10} is the innermost layer and I_{n1} is the outermost layer, which directly faces the environment. For internal neighboring layers, we have

$$I_{(i-)0} = I_{i1} \quad (2 < i < n) \tag{1}$$

Variable *Contact* is defined to describe the contact situation at (inter-) boundaries for layer *i;* the contact situations determine the heat and moisture transfer behavior at boundaries between layers:

$$Contact_{in} = \begin{cases} 1 & I_{ij} = 0 \\ 0 & I_{ij} \neq 0 \end{cases} \quad (1 \leq i \leq n,\ j = 0, 1) \tag{2}$$

3. Each layer consists of more than one type of fiber, which is characterized by the fractional proportion f_{ti} for each the fiber type t_i, and t_n is the total number of types of textile in the layer.
4. Possible physical properties p_{ti} of the fiber t_i are listed in Table I; the weighted averaged property $\bar{p}$ is used based on their type fractions f_{ti}, and is expressed as

$$\bar{p} = \sum_{ti=1}^{tn} f_{ti} p_{ti} \quad (tn \geq 2) \tag{3}$$

This assumption shall be accurate at the first order because the physical processes occurring round the fibers and/or in the fibers are primarily dependent on the physical properties of the hosting fibers. Inside

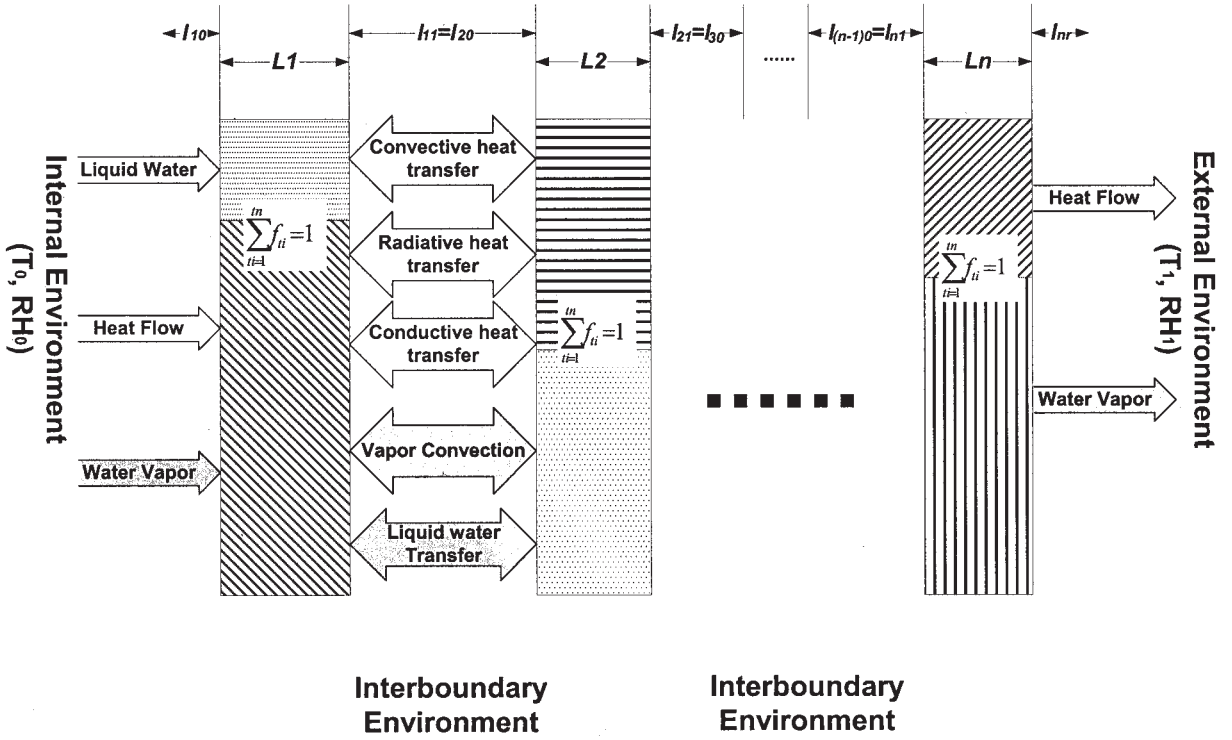

Figure 1 Schematic diagram for MLMM model.

each layer, the dynamic moisture sorption process and the affected dynamic thermal statuses of each type of fiber listed in Table I are calculated separately on the basis of their own properties. The calculated results are averaged and used in the mathematical model.

Governing equations

On the basis of the above assumptions and the governing equations for the single-layer isotropic model, the governing equations for each layer in the multilayer anisotropic model could be expressed as

Moisture vapor balance

$$\frac{\partial(C_a\varepsilon_a)}{\partial t}=\frac{1}{\tau_a}\frac{\partial}{\partial x}\left[D_a\frac{\partial(C_a\varepsilon_a)}{\partial x}\right]-\varepsilon_f\xi_l\overline{\Gamma}_f+\overline{\Gamma}_{lg} \quad (4)$$

Moisture liquid balance

$$\frac{\partial(\rho_l\varepsilon_l)}{\partial t}=\frac{1}{\tau_l}\frac{\partial}{\partial x}\left\{\sum_{ti=1}^{tn} f_{ti}[D_l(\varepsilon_l)]_{ti}\left[\frac{\partial(\rho_l\varepsilon_l)}{\partial x}\right]_{ti}\right\}-\varepsilon_f\xi_2\overline{\Gamma}_f-\overline{\Gamma}_{lg} \quad (5)$$

Heat balance

$$\overline{c}_v\frac{\partial T}{\partial t}=\frac{\partial}{\partial x}\left[\overline{K}_{\mathrm{mix}}(x)\frac{\partial T}{\partial x}\right]+\frac{\partial F_R}{\partial x}-\frac{\partial F_L}{\partial x}+\varepsilon_f\overline{\Gamma}_f(\xi_1\overline{\lambda}_v+\xi_2\overline{\lambda}_l)-\lambda_{lg}\overline{\Gamma}_{lg} \quad (6)$$

In eq. (5), the process of liquid transfer in the area with different capillary capabilities is calculated through the $\sum_{ti=1}^{tn} f_{ti}[D_l(\varepsilon_l)]_{ti}[\partial(\rho_l\varepsilon_l)/\partial x]_{ti}$, where $[D_l(\varepsilon_l)]_{ti}$ is the

TABLE I
Linearly Averaged Variables

Property	Dynamic property	Dynamic status
Fiber radius	Heat of fiber moisture sorption	Fiber moisture concentration
Fiber emissivity	Fiber specific heat	Fiber moisture sorption rate
Fiber radiation absorption constant		Liquid moisture volumetric fraction
Thermal conductivity		

liquid diffusivity for the liquid transfer in the areas of fiber type *ti*, and is calculated by eq. (7), which was derived in Li et al.[11] When the fiber type *ti* is hydrophobic, the contact angle θ is an obtuse angle, and eq. (7) will yield a negative value, indicating that the liquid could not be transferred by capillary force. Therefore, when this happens, the $[D_l(\varepsilon_l)]_{ti}$ is forced to be zero.

$$D_l(\varepsilon_l) = \frac{\gamma \cos\theta \sin^2\alpha d_c \varepsilon_l^{1/3}}{20\eta\varepsilon^{1/3}} \tag{7}$$

where the $\bar{c}_v$, $\lambda_{(v,l)}$, $\bar{K}_{\text{mix}}$ in eq. (6) are the dynamical average volumetric specific heat, heat of sorption, and thermal conductivity, respectively. They are defined by eq. (8) to (10).

$$\bar{c}_v = \varepsilon_l c_{vl} + \varepsilon_f \bar{c}_{vf} + \varepsilon_a c_{va}$$

$$\bar{c}_{vf} = \sum_{ti=1}^{tn} f_{ti}(c_v)_{ti} \tag{8}$$

$$\bar{\lambda}_{(v,l)} = \sum_{ti=1}^{tn} f_{ti}[\lambda_{(v,l)}]_{ti} \tag{9}$$

$$K_{\text{mix}} = \varepsilon_l K_l + \varepsilon_f \bar{K}_f + \varepsilon_a K_a$$

$$\bar{K}_f = \sum_{ti=1}^{tn} f_{ti}(K_f)_{ti} \tag{10}$$

The dynamic average moisture sorption rate $\bar{\Gamma}_f$ and mean water content of fibers $\bar{W}_{cf}$ are expressed as

$$\bar{\Gamma}_f = \sum_{ti=1}^{tn}\left[f_{ti}\left(\frac{\partial C_f}{\partial t}\right)_{ti}\right] = \sum_{ti=1}^{tn} f_{ti}\left\{\frac{1}{r_{ti}}\frac{\partial}{\partial r_{ti}}\left[r_{ti}(D_f)_{ti}\frac{\partial C_f}{\partial r}\right]\right\}_{ti} \tag{11}$$

$$\bar{W}_{cf} = \sum_{ti=1}^{tn} f_{ti}(W_{cf})_{ti} = \sum_{ti=1}^{tn} f_{ti}\frac{(C_f)_{ti}}{(\rho_f)_{ti}} \tag{12}$$

The dynamic average moisture condensation/evaporation sorption rate $\bar{\Gamma}_{lg}$ is determined by the distribution of the liquid transfer capabilities in the fabric, and therefore can be expressed as

$$\bar{\Gamma}_{lg} = \sum_{ti=1}^{tn} [f_{ti}(\Gamma_{lg})_{ti}] \tag{13}$$

For the process of thermal radiation, we have[8]

$$\frac{\partial F_R}{\partial x} = -\bar{\beta}F_R + \bar{\beta}\sigma T^4 \tag{14}$$

$$\frac{\partial F_L}{\partial x} = \bar{\beta}F_L - \bar{\beta}\sigma T^4 \tag{15}$$

$$\left.\begin{aligned} \bar{\beta} &= \frac{(1-\varepsilon)}{\bar{r}}\bar{\varepsilon}_r \\ \bar{r} &= \sum_{ti=1}^{tn} f_{ti} r_{ti} \\ \bar{\varepsilon}_r &= \sum_{ti=1}^{tn} f_{ti}(\varepsilon_r)_{ti} \end{aligned}\right\} \tag{16}$$

Boundary and interboundary conditions

As shown in Figure 1, there are mass and heat exchanges between the layers at the (inter-) interfaces as well as the boundaries facing onto both internal and external environments. Wang et al.[9] reported that significant influences on the heat and moisture transfer behaviors inside the fabric system arise from waterproof fabrics (WPF) that are bonded at the boundaries. Therefore, according to the contact status (contact and noncontact) and waterproof fabric existence (with, without) at fabric (inter-) interfaces (inner side and outer side) for each layer, a total of eight boundary condition situations need to be considered for the liquid water, moisture vapor, and heat transfer processes. The (inter-) boundary conditions are summarized in Table II.

H_{mn} and H_{cn} (n = 0, 1) in eq. (17) and (18) are the combined mass transfer and the combined heat transfer coefficients. If there is a layer of WPF at the boundaries, which would increase the thermal and moisture transfer resistance, H_{mn} and H_{cn} can be expressed as eq. (19), where W_n and R_n are the resistances of the moisture vapor and heat transfer of the surfaces of the fabric, h_{mn} and h_{cn} are the mass and heat transfer coefficients of the internal (n = 0) and the external environment (n = 1), respectively.[9]

$$H_{mn} = 1/(W_n + 1/h_{mn}) \tag{19a}$$

$$H_{cn} = 1/(R_n + 1/h_{cn}) \tag{19b}$$

According to Figure 1, the environmental boundaries of the inner and the outer side of each fabric layer are denoted by subscripts (0*B*) and (1*B*). The environmental status for each fabric layer are described by the physical variable groups (T, RH, ε_l) or (T, C_a, ε_l).

TABLE II
Boundary Conditions for Heat and Moisture Transfer for Each Fabric Layer

	Inner side	
Noncontact		
Without WPF	$D_a\,\partial\dfrac{\delta(C_a\varepsilon_a)}{\delta x}\Big\vert_{x=0} + H_{m0}(C_{0B} - C_{a0}) = 0$	
	$\rho_l D_l\,\partial\dfrac{\delta\varepsilon_l}{\delta x}\Big\vert_{x=0} + \dfrac{\varepsilon_l}{\varepsilon}h_{lg}(C_{0B} - C^*) = 0$	
	$K_{\text{mix}}\dfrac{dT}{dx}\Big\vert_{x=0} + H_{c0}(T_{0B} - T_0) + \lambda_{lg}\dfrac{\varepsilon_l}{\varepsilon}h_{lg}(C_{0B} - C^*) = 0$	(17a)
With WPF	$D_a\,\partial\dfrac{\delta(C_a\varepsilon_a)}{\delta x}\Big\vert_{x=0} + H_{m0}(C_{0B} - C_{a0}) = 0$	
	$\rho_l D_l\,\partial\dfrac{\delta\varepsilon_l}{\partial x}\Big\vert_{x=0} = 0$	
	$K_{\text{mix}}\dfrac{dT}{dx}\Big\vert_{x=0} + H_{c0}\,(T_{0B} - T_0) + \lambda_{lg}\dfrac{\varepsilon_l}{\varepsilon}h_{lg}(C_{0B} - C^*) = 0$	(17b)
Contact		
Without WPF	$(C_a\varepsilon_a) = (C_{0B}\varepsilon_a)$	
	$\varepsilon_{l0} = \varepsilon_{l0B}$	
	$T = T_{0B}$	(17c)
With WPF	$D_a\dfrac{\partial(C_a\varepsilon_a)}{\partial x}\Big\vert_{x=0} + H_{m0}(C_{0B} - C_{a0}) = 0$	
	$\rho_l D_l\dfrac{\partial\varepsilon_l}{\partial x}\Big\vert_{x=0} = 0$	
	$T = T_{0B}$	17d)
	Outer side	
Noncontact		
Without WPF	$-D_a\dfrac{\partial(C_a\varepsilon_a)}{\partial x}\Big\vert_{x=1} + H_{ml}(C_{1B} - C_{aN}) = 0$	
	$-\rho_l D_l\dfrac{\partial\varepsilon_l}{\partial x}\Big\vert_{x=1} + \dfrac{\varepsilon_1}{\varepsilon}h_{lg}(C_{1B} - C^*) = 0$	
	$-K_{\text{mix}}\dfrac{dT}{dx}\Big\vert_{x=1} + H_{c1}(T_{NB} - T_N) + \dfrac{\varepsilon_l}{\varepsilon}\lambda_{lg}h_{lg}(C_{1B} - C^*) = 0$	(18a)
With WPF	$-D_a\dfrac{\partial(C_a\varepsilon_a)}{\partial x}\Big\vert_{x=L} + H_{m1}(C_{1B} - C_{aN}) = 0$	
	$\rho_l D_l\dfrac{\partial\varepsilon_l}{\partial x}\Big\vert_{x=L} = 0$	
	$-K_{\text{mix}}\dfrac{dT}{dx}\Big\vert_{x=L} + H_{c1}(T_{NB} - T_N) = 0$	(18b)
Contact		
Without WPF	$(C_a\varepsilon_a) = (C_{1B}\varepsilon_a)$	
	$\varepsilon_{lN} = \varepsilon_{l1B}$	
	$T = T_{1B}$	(18c)
With WPF	$-D_a\dfrac{\partial(C_a\varepsilon_a)}{\partial x}_{x=L} + H_{m1}(C_{1B} - C_{aN}) = 0$	
	$\rho_l D_l\dfrac{\partial\varepsilon_l}{\partial x}\Big\vert_{x=L} = 0$	
	$T = T_{1B}$	(18d)

EXPERIMENTAL

The experiment simulating infant bed-wetting process during sleep was designed to investigate the process of coupled heat and moisture (water vapor and liquid water) transfer through the multiple-layered fabric assembly, and the experimental result was used to validate the mathematical model developed. The key output physical variables include dynamic temperature distribution across the fabric system, dynamic moisture vapor/relative humidity (RH) concentration distribution across the fabrics system, and dynamic liquid water volume distribution.

TABLE III
Specifications of Fabric Assemblies

Fabric assembly				
	COMP			COTN
No. of layers	4			4
Thickness (mm)	6.60 ± 0.05			6.88 ± 0.02
Fabric construction	1 polypropylene–cotton fabric (pcf) 3 cotton fabrics (cot-A)			1 cotton fabrics (cot-B) 3 cotton fabrics (cot-C)
Specification of individual fabrics				
	pcf	cot-A	cot-B	cot-C
Thickness (mm)	0.93 ± 0.05	1.88 ± 0.04	0.98 ± 0.04	1.89 ± 0.07
Fiber type	Polypropylene/cotton	Cotton	Cotton	Cotton
Area density (g cm^{-2})	0.015	0.052	0.015	0.029
Porosity	0.82	0.82	0.80	0.80
Composition	75% polypropylene and 25% cotton	100% cotton	100% cotton	100% cotton

Four-layer fabric assemblies

Two 4-layer fabric assemblies were used. One consisted of four single layers of cotton fabrics (COTN); the other consisted of three single layers of cotton fabric and a layer of double-sided polypropylene–cotton fabric (COMP). This special composite fabric possessed one-way liquid water transfer capability.[10] The COTN assembly represents the traditional isotropic cotton bedding system used in hospitals and homes, whereas the COMP assembly is a newly designed bedding system that has anisotropic polypropylene–cotton composite structure. The fabric specifications are listed in Table III. For each fabric assembly, five samples (size 9×9 cm^2) were prepared and tested in the experiments. Fabrics were fixed solidly in a G-type clip and conditioned in the testing room for 24 h to ensure good contact between layers.

Setup

In this experiment, the liquid transfer capability of the fabrics and the water content distribution in the fabrics were measured by using an instrument called moisture management tester (MMT).[10] The dynamic distribution of temperature and humidity across the fabric were measured by using a computer-interfaced data-acquisition system equipped with temperature and humidity sensors. The experimental setup is shown in Figure 2.

The layered fabric assembly is placed between the two sensor panels, designed to detect the present of liquid water at both the top and the bottom of the fabric assembly.[10] Three pairs of temperature and humidity sensors are inserted between the intersurfaces among layers 1, 2, 3, and 4. All sensors are connected to a computer-interfaced monitoring system, through which the data sampling of temperature and relative humidity is continuously recoded during the experiments. The liquid water was introduced from the top using a plastic tube, with which the volume of liquid can be controlled through a computer-controlled pump.

Protocol

The experiment was carried out in a climate chamber conditioned as at T = 25°C, RH = 65%. The experiment for each sample consisted of three stages, lasting for 5 min, to simulate the bed-wetting process:

- In the first 25 s (~0.45 min), the sampling system continues to record the fabric thermal and moisture status without the presence of liquid water.
- In the second stage, 30 mL liquid water with temperature of 36°C is introduced to the top surface of the assembly sample in 45 s (0.75 min),

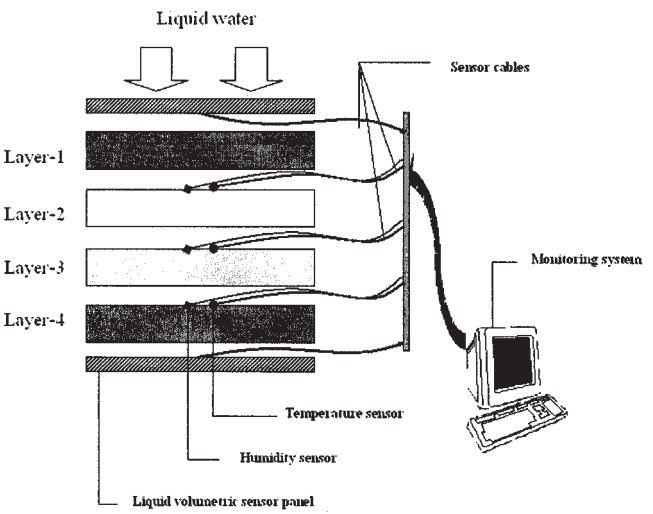

Figure 2 Experimental setup.

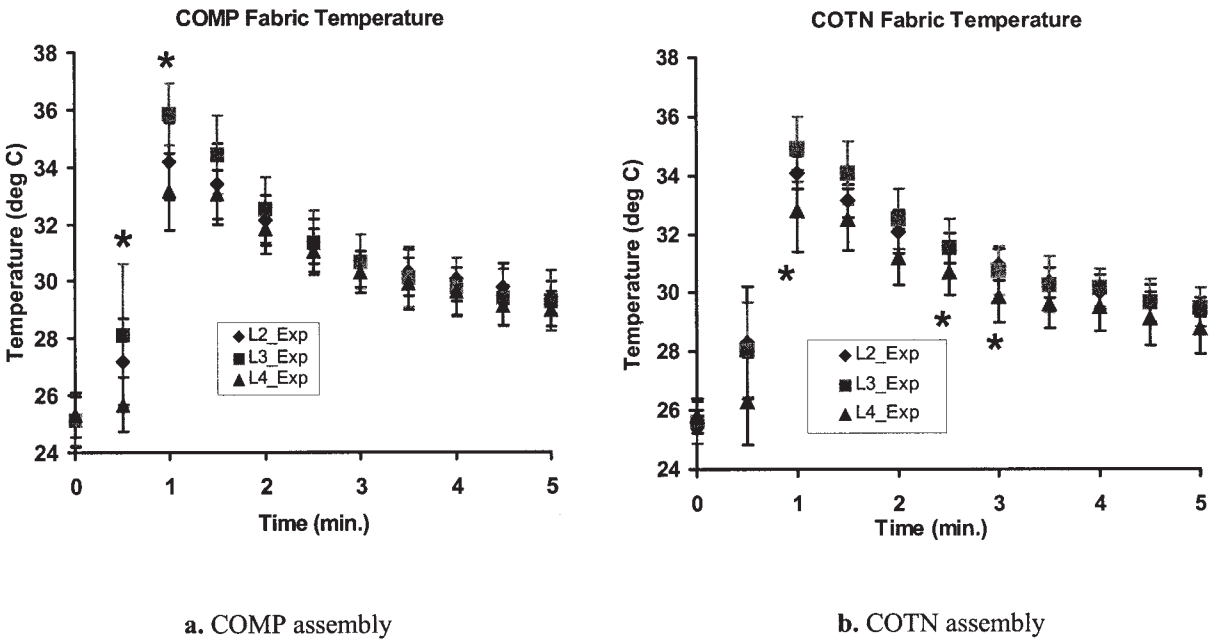

a. COMP assembly **b.** COTN assembly

Figure 3 Dynamic temperature profile for layered fabrics: (a) COMP assembly; (b) COTN assembly. Note: Positions marked with an asterisk indicate significant differences are found in the temperatures among layers at $p < 0.05$.

after which the liquid water diffuses into the system of fabrics by capillary action and gravity. The dynamic change of temperature, humidity across the sample, and the liquid water at both top and bottom fabric surfaces are continuously recorded by temperature/humidity sensors located at the intersurfaces and the liquid water–sensing panels at both top and bottom surfaces.

- The data-acquisition system continues to record for the duration of the experiment.

RESULTS AND DISCUSSION

The experimental results include dynamic temperature and humidity profiles at different positions between the fabric layers, and the difference of liquid

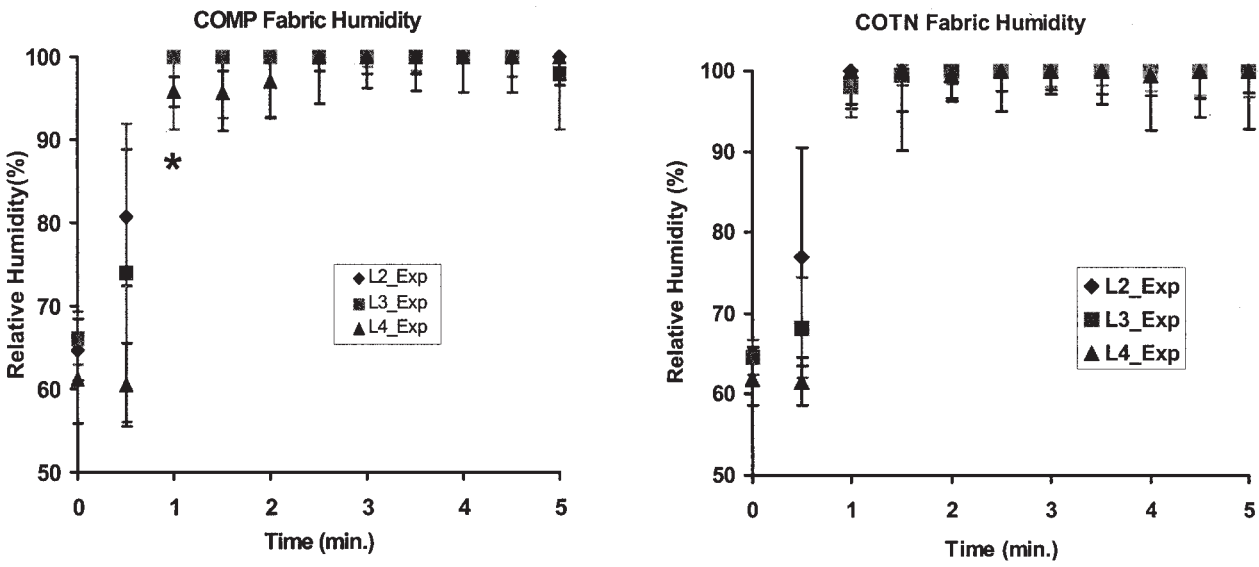

a. COMP assembly **b.** COTN assembly

Figure 4 Dynamic RH profile for layered fabrics: (a) COMP assembly; (b) COTN assembly. Note: Positions marked with an asterisk indicate significant differences are found in the RH among layers at $p < 0.05$.

TABLE IV
Simulation Parameters

Experimental protocol			
	Stage 1	Stage 2	Stage 3
Time duration (min)	0.45	0.75	4.8
Top environment	25°C, 65%	36°C, 100%	25°C, 65%
Bottom environment	25°C, 65%	25°C, 65%	25°C, 65%
Contact situation	(1, 1, 1, 1, 1, 1, 1, 0)	(1, 1, 1, 1, 1, 1, 1, 0)	(0, 1, 1, 1, 1, 1, 1, 0)

Calculation parameters		
Transfer coefficients at outermost boundaries	Layer 1, outer top boundary (L1, 0)	Layer 4, outer bottom surface (L4, 1)
h_{mn} ($m\ s^{-1}$)	0.2×10^{-3}	0.2×10^{-3}
h_{cn} ($W\ m^{-2}\ K$)	10.0	10.0

Fabric constructional parameters				
	COMP		COTN	
	(Material, type fraction f_a)	Capillary radius with the maximum distribution inside the fabric d_c (m)[11]	(Material, type fraction f_a)	Capillary radius with the maximum distribution inside the fabric d_c (m)[11]
Layer 1	(Polypothylene, 75%) (Cotton, 25%)	200×10^{-6}	(Cotton, 100%)	200×10^{-6}
Layer 2				
Layer 3	(Cotton, 100%)		(Cotton, 100%)	
Layer 4				

Fiber physical parameters			
Property	Symbol	Polypothylene	Cotton
Density,[12] (kg m^{-3})	ρ	0.91×10^3	1.52×10^3
Radius	R_f	0.96×10^{-5}	1.03×10^{-5}
Diffusion coefficient of vapor in the fiber,[13] m^2 s	D_f	1.34×10^{-13}	5.8×10^{-13}
Heat of moisture sorption,[14] (kJ kg^{-1})	λ_v	2522.0	$2522.0 + 1602.5e^{-11.72W_{cf}}$
Volumetric heat capacity of fiber,[11] kJ $m^{-3}\ K^{-1}$	c_{vf}	$4.184 \times 10^3 \times 0.91 \times \frac{0.32 + W_{cf}}{1.0 + W_{cf}}$	$4.184 \times 10^3 \times 1.52 \times \frac{0.32 + W_{cf}}{1.0 + W_{cf}}$
Contact angle of liquid water[13]	ϕ	135°	85°
Emissivity,[15]	ε_t	0.9	0.9
Radiative absorption constant,[8] m^{-1}	β	$\beta = \frac{(1 - \varepsilon_i)}{r_i}\varepsilon_{ri}$ $(i = 1, 2, 3, 4)$	

water volumetric fraction at the top surface of the fabric assembly when the system reached the steady state.

Dynamic temperature distribution

Figure 3 shows the dynamic distribution of the temperature across the layered fabrics: (a) COMP and (b) COTN. For both fabrics, similar features are found in the dynamic temperature distributions:

1. Because of the quick transport of the liquid water with higher temperature, the temperatures at the top of layers 2, 3, and 4 increase from an initial 25°C to the higher range of 34–38°C in the first two stages, and then decrease steadily to 30°C at the end of the third stage. The decrease in temperature is mainly attributed to the convective loss to the environment when there is no further warm liquid water added.
2. Because of the moisture sorption inside the fabrics along the experimental process, the temperature of layer 3 tends to increase to the highest level in all three layers within the first minute. Then the increased thermal conductivity of the fabric attributed to the liquid occupation causes the temperature differences of the three layers to decrease gradually.

To determine whether there is significant difference between the temperatures of different layers, the *t*-test for temperatures of layer 2 and layer 3, layer 2 and layer 4 were performed every 0.5 min. For the COMP assembly, there were significant differences between

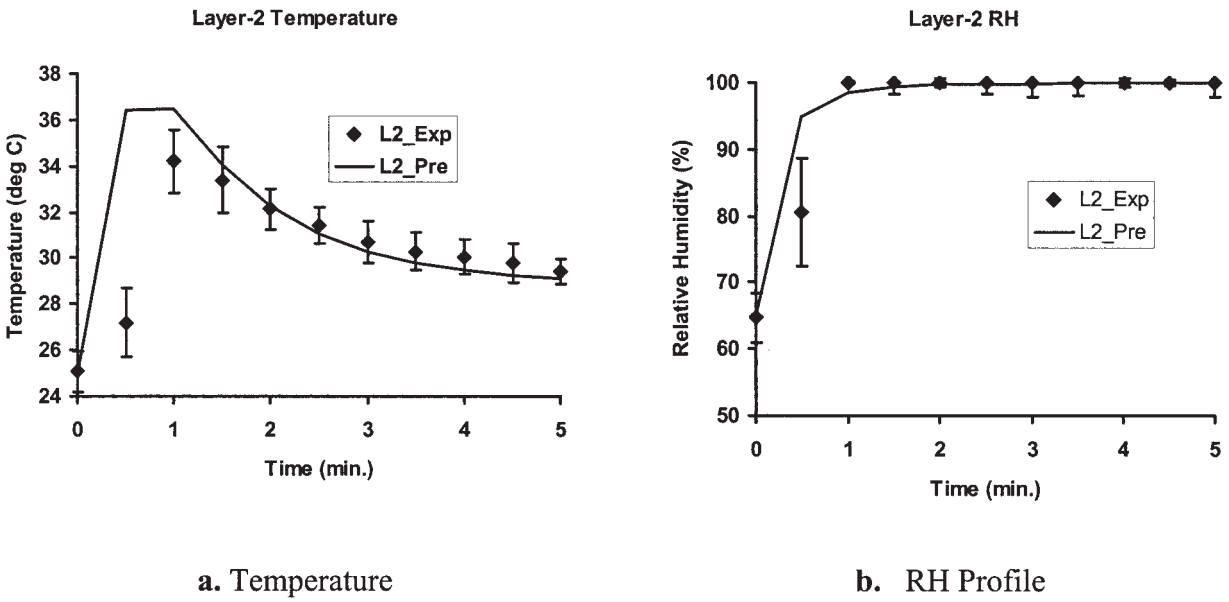

Figure 5 Layer 2 temperature (a) and RH profiles (b) for the COMP assembly.

layer 2 and layer 4 at 0.5 min ($p < 0.05$) and layer 2 and layer 3 at 1.0 min ($p < 0.05$). For the COTN assembly, there were significant differences of temperature between layer 2 and layer 4 at 1.0, 2.5, and 3.0 min ($p < 0.05$), as shown in Figure 3(b).

Overall during the entire experiment, there was no significant temperature difference for each fabric layer. This is possibly because of the quick transfer of liquid water from the top surface to the bottom surface. The thermal effect from moisture vapor sorption is weakened by the fast increased thermal conductivity of the fabric resulting from the liquid diffusion, which decreases the temperature differences between layers.

Dynamic humidity distribution

The dynamic distributions of the relative humidity (RH) across the layered fabrics are shown in Figure 4: (a) COMP and (b) COTN. For both fabrics, features similar to those in the dynamic mean RH distribution were observed:

1. Because of the quick and transport of the liquid water, the RH at the top of layers 2, 3, and 4 increases from 65 to 100%, initially, and then remains at the saturated level until completion of the experiment.
2. The time sequence for each layer approaching the 100% level takes the sequence of layer 2,

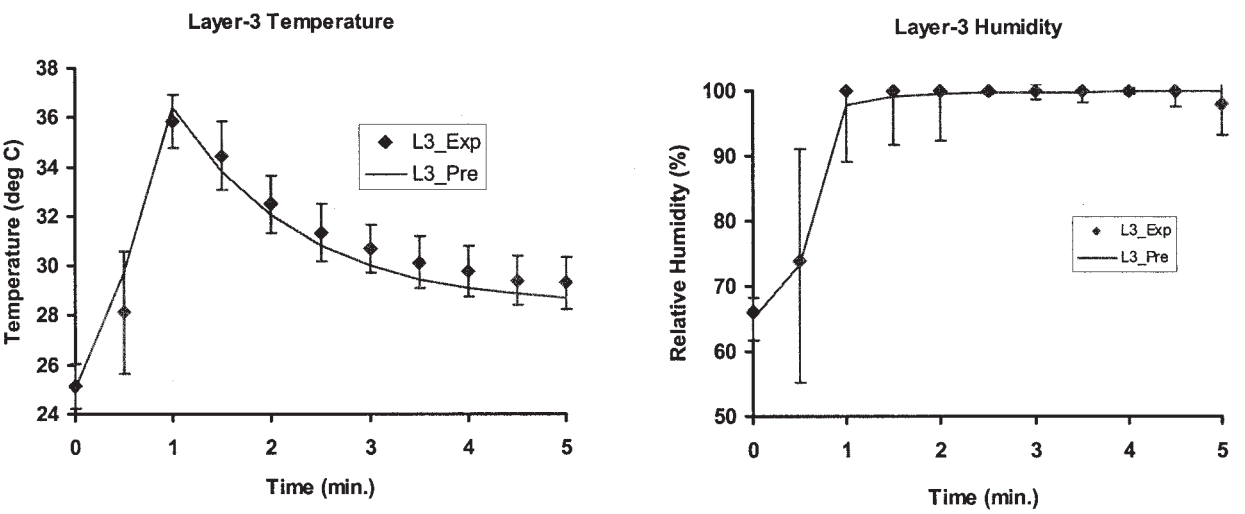

Figure 6 Layer 3 temperature (a) and RH profiles (b) for the COMP assembly.

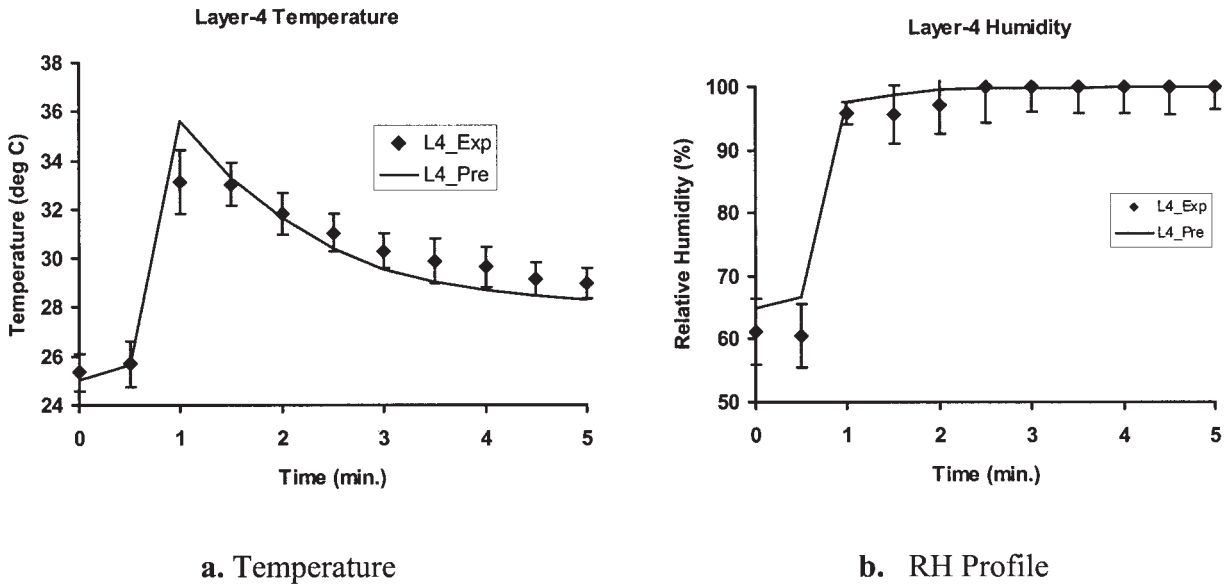

Figure 7 Layer 4 temperature (a) and RH profiles (b) for the COMP assembly.

layer 3, and layer 4, alone with diffusion of liquid water.

To determine whether there were significant differences in relative humidity between different layers, *t*-tests for the mean RH between layer 2 and layer 3, and layer 4 were performed every 0.5 min. For the COMP assembly there were significant differences between layer 2 and layer 4 at 1.0 min ($p < 0.05$), as shown in Figure 4(a). No significant difference in RH was found for the COTN assembly. Similar to the temperature distributions, there were no significant differences in RH between fabric layers during the experiments because of the quick transfer of liquid water from the top surface to the bottom surface.

Numerical simulation

Simulation configuration

Numerical simulations were carried out for the experiments by using the developed mathematical models. According to the experiment, the simulations were performed in three stages with different environmental conditions. The contact situations between layers are defined as *Contact* (1). The contact situation for the

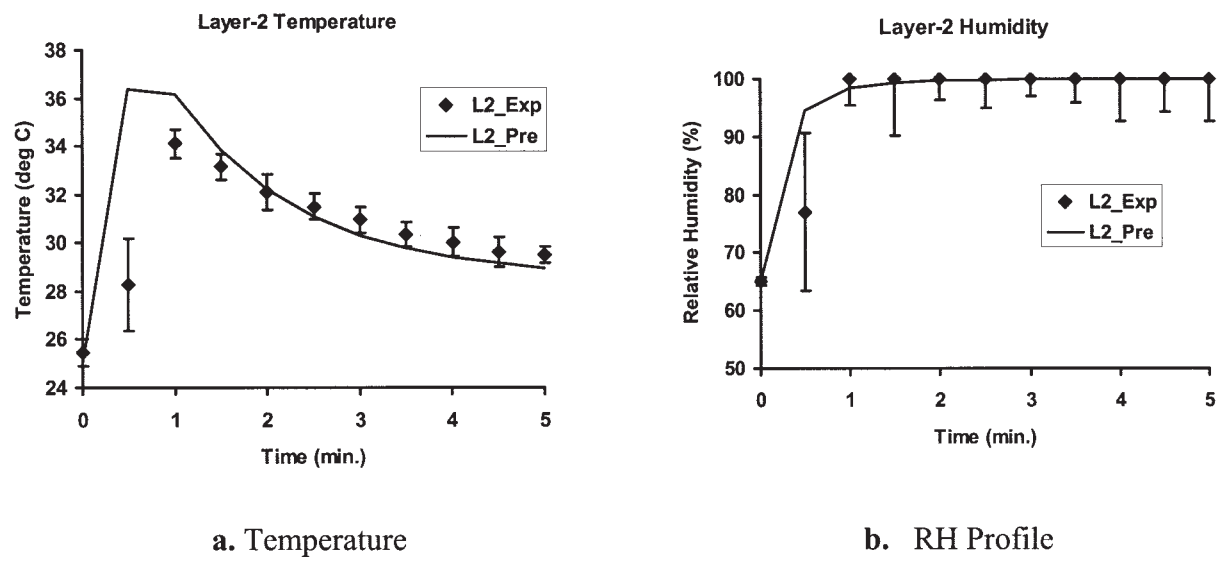

Figure 8 Layer 2 temperature (a) and RH profiles (b) for the COTN assembly.

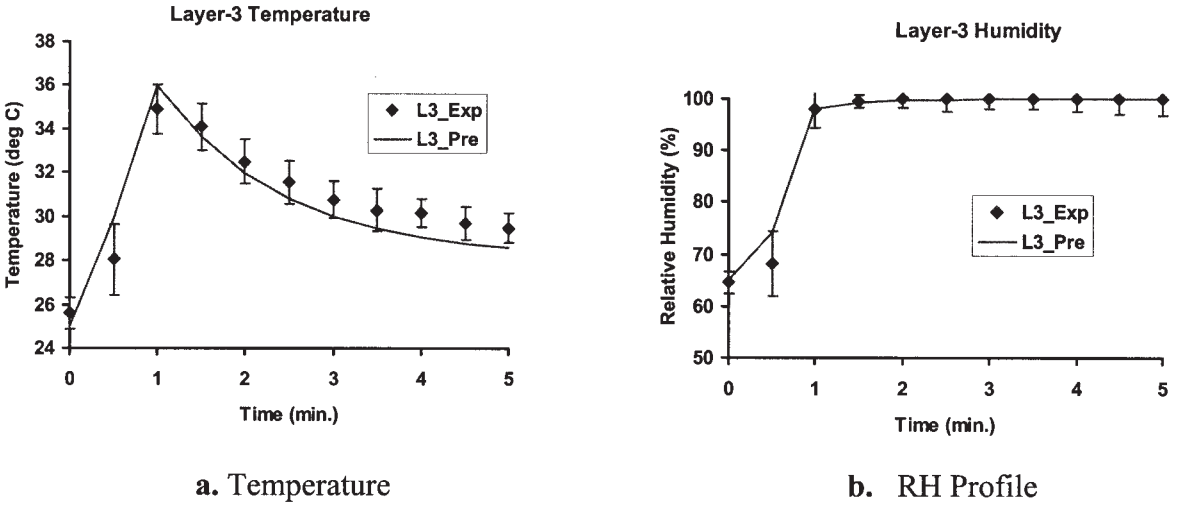

Figure 9 Layer 3 temperature (a) and RH profiles (b) for the COTN assembly.

outermost boundaries are defined as *Contact* (1) or *Apart* (0). The detailed parameters are listed in Table IV.

Comparisons between computational and experimental results

Dynamic temperature and RH profiles in different layers. To illustrate the comparison between the computational and experimental results clearly, we plotted the dynamic temperature and RH profiles for each layer (layers 2, 3, and 4) separately. Figures 5 to 7 and Figures 8 to 10 are the comparisons for COMP assemblies and COTN assemblies, respectively. These figures show that for both COMP and COTN assemblies, the predicted layered temperature and RH of each layer agree well with the experimental results; the predicted values almost all fall in the range of standard deviation of the experimental values, except in the first 0.5 min at layer 2. In this case, the predicted RH tends to increase faster than the experimental measurements, which may be attributable to the assumption of perfect contact in the numerical simulation between skin and the fabric. This may not be the case under experimental conditions.

Final liquid volume at the fabric top surface. Figure 11 shows the comparison of liquid volumetric fraction (LVF) at the top and bottom surfaces at the end of the experiment for the COMP and COTN assemblies. The LVF at the bottom surface of both assemblies at the end of the experiment reached, 0.80 and 0.82 for the COTN and COMP assemblies, respectively. At the top surface, because of the gravity and liquid water transfer capability effect of the liquid water, the LVF values for the two assemblies are significantly different (p

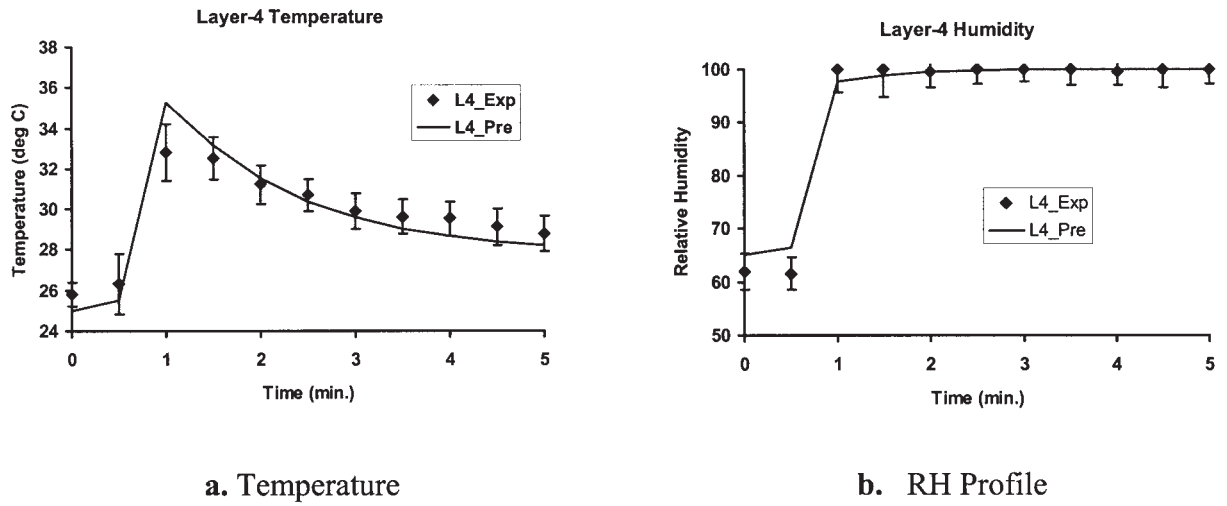

Figure 10 Layer 4 temperature (a) and RH profiles (b) for the COTN assembly.

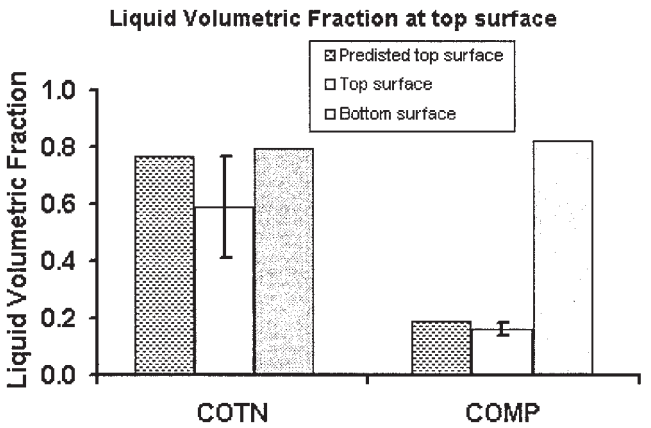

Figure 11 Comparison of the final LVF at the top surface.

< 0.001): 0.60 and 0.16 for the COTN and COMP assemblies, respectively. The calculated final LVF at the top surface is 0.21 for the COMP assembly and 0.78 for the COTN assembly, all within the range of error bars of the experimental value, indicating that good agreement was obtained.

Figure 12 shows the simulated dynamic distribution of LVF across the fabric layers during the liquid transfer process for: (a) the COMP assembly and (b) the COTN assembly. There are some similar features for both fabrics. For both COMP and COTN assemblies, from the second stage, liquid water is presented and transferred very quickly to layer 4. The time that liquid water is transferred from layer 1 to layer 4 is about 6 s for both cases. The LVF inside the fabric distributes evenly at each layer, varying only slightly for the duration of the experiment.

Further discussion

Besides the measured physical parameters, the simulation can provide further information on dynamic heat and moisture transfer processes in the fabric and fibers across the assembly, which are shown and discussed in this section.

Heat and moisture transfer through the fabric

Figures 13 and 14 show the dynamic temperature and moisture vapor concentration distributions across the fabric thickness for: (a) the COMP assembly and (b) the COTN assembly. The two cases have similar distribution patterns of temperature and moisture vapor concentration, possibly because cotton fibers are used as the main material for the two fabric assemblies.

Fabric moisture sorption process

Figures 15 to 17 show the dynamic RH distribution, dynamic mean fiber water content, and dynamic mean fiber moisture sorption rate of each layer across the fabric thickness for: (a) the COMP assembly and (b) the COTN assembly. The two cases have similar RH distributions but significantly different distributions of fiber water content and fiber moisture sorption rate.

For the COMP assembly, the top layer fabric consists of hygroscopic cotton and nonhygroscopic polypropylene fibers with type fractions of 25 and 75%. Therefore, according to eqs. (12) and (13), the dynamic mean fiber water content and fiber moisture sorption rate of the fibers the in first layer are about 75% lower than those in both the other three cotton fabric layers and the layers in the COTN assembly.

Fiber moisture sorption for composite fibers

For the COMP assembly, the dynamic mean fiber moisture concentration, moisture sorption rate, and

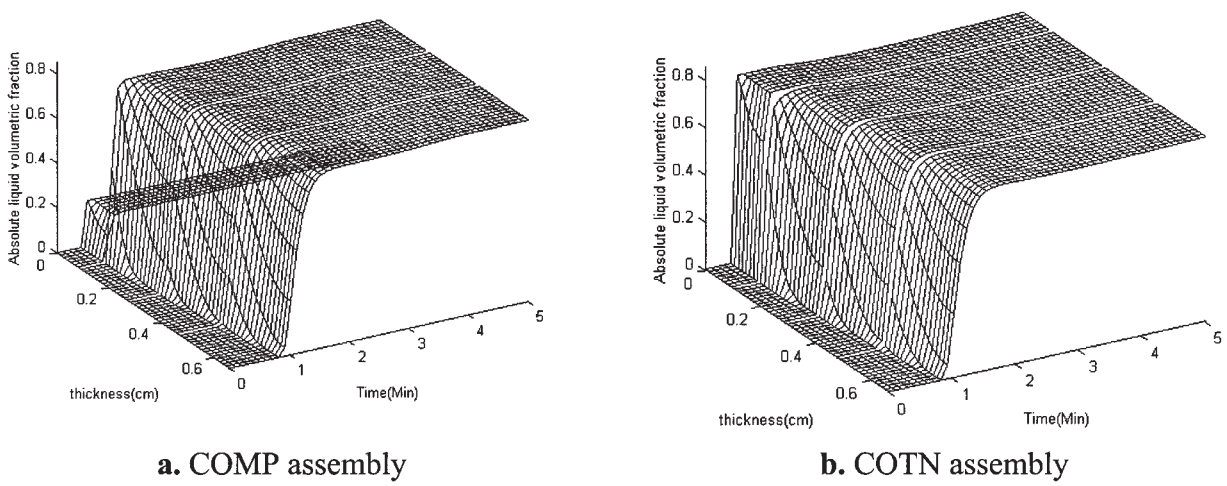

Figure 12 Dynamic ALVF transfer for the layered fabrics: (a) COMP assembly; (b) COTN assembly.

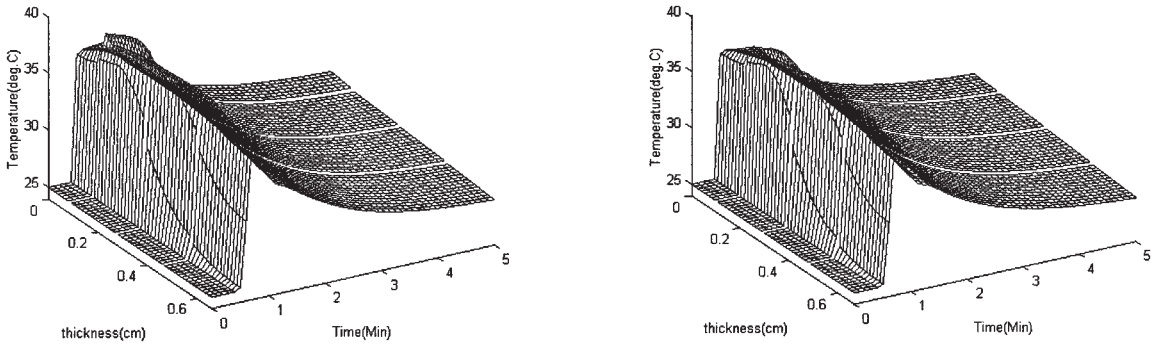

Figure 13 Dynamic temperature distribution for the layered assemblies: (a) COMP; (b) COTN.

the fiber water content in the first layer are shown separately in Figures 18 and 19 for: (a) the polypropylene fibers and (b) the cotton fibers. Using the same axes scales, the differences of the moisture sorption capability between the two types of fiber are clearly illustrated. There is almost no sorption process occurring for the polypropylene fibers. For cotton fibers, however, it has a profile similar to that of cotton fibers in layer 2 to layer 4, as well as the cotton fibers in the COTN assembly.

CONCLUSIONS

In summary, a new model has been developed on the basis of the previous isotropic models, taking into account the influence of different materials in each layer of fabrics. In the new model, the governing principles and equations of heat and moisture transfer inside each layer are the same as those in the isotropic model. Influences of different fiber types in each layer are considered and different internal interfaces between each layer are developed. The model was validated by physical experiments using fabric assemblies with different liquid transfer properties and multiple fiber types with different moisture sorption capabilities. The comparisons between the calculated and experimental results show the new model can describe the coupled heat and moisture (vapor and liquid) transfer in the multilayer anisotropic fabric assembly with good accuracy. Significant influences of different fabrics made of different types of fibers in the assembly were illustrated through the simulation. The new model enhances the functional flexibilities and provides more comprehensive information for analyzing the mechanisms of coupled heat and moisture (vapor and liquid) through the layered fabric assemblies with more complex structural features.

The authors thank the Hong Kong Research Grant Committee and the Hong Kong Polytechnic University for funding this research through projects PolyU5111/98E, PolyU5151/01E, and A188.

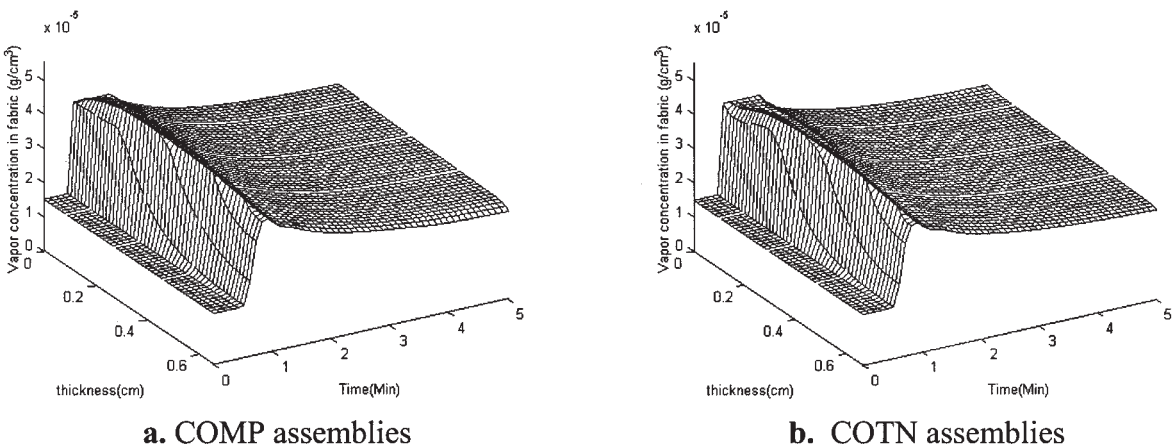

Figure 14 Dynamic water vapor concentration distribution for the layered assemblies: (a) COMP; (b) COTN.

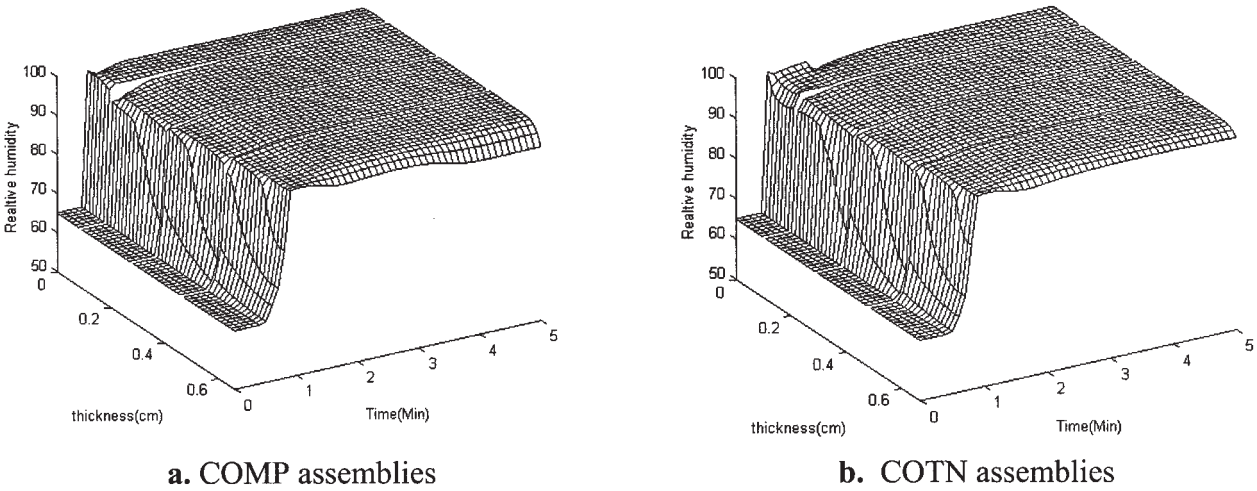

Figure 15 Dynamic RH distribution for the layered assemblies: (a) COMP; (b) COTN.

NOMENCLATURE

Symbol abbreviation	description
C*	saturated water vapor concentration in the air of the fabric, kg m^{-3}
C_a	water vapor concentration . . .
C_{env}	water vapor concentration of the ambient air, kg.m^{-3}
C_f	water concentration in the fibers of the fabric, kg.m^{-3}
C_{fs}	water vapor concentration at the fiber surface, kg.m^{-3}
$Contact_{in}$	contact situation with the neighbored layer for the layer i (n = 0, left side; n = 1, right side)
c_v	volumetric heat capacity of the fabric, kJ m^{-3} K^{-1}
c_{va}	volumetric heat capacity of the air, kJ m^{-3} K^{-1}
c_{vf}	volumetric heat capacity of the fiber, kJ m^{-3} K^{-1}
c_{vl}	volumetric heat capacity of the liquid water, kJ m^{-3} K^{-1}
D_a	diffusion coefficient of water vapor in the air of the fabric, m^2 s^{-1}
D_f	diffusion coefficient of water vapor in the fibers of the fabric, m^2 s^{-1}
D_l	diffusion coefficient of liquid water in the fabric, m^2 s^{-1}
F_L	elementary total thermal radiation incident inside the clothing traveling to the left, W m^{-2}
F_R	elementary total thermal radiation incident inside the clothing traveling to the right, W m^{-2}
f_{ti}	fraction of fiber type ti in a layer of fabric
h_{cn}	convective heat transfer coefficient at the clothing surface (n = 0, inner surface; n = 1, outer surface), W m^{-2} K^{-1}

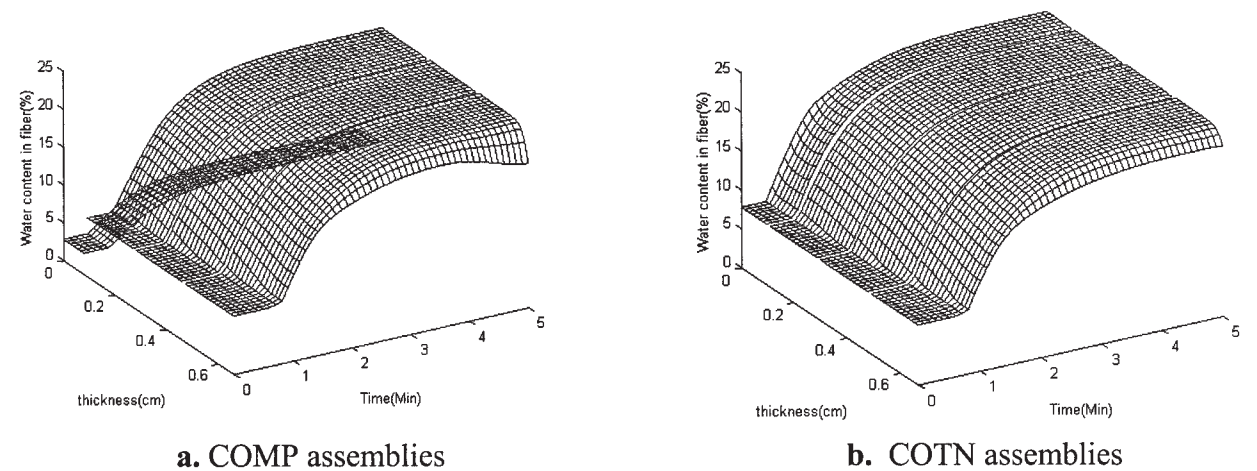

Figure 16 Dynamic mean fiber water content in each layer for the layered assemblies: (a) COMP; (b) COTN.

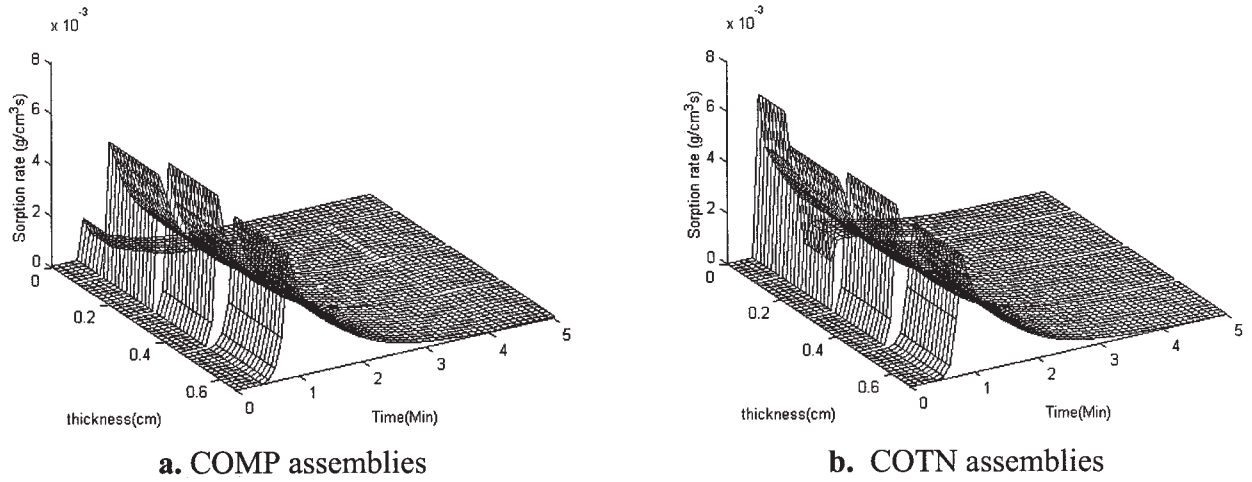

Figure 17 Dynamic mean fiber moisture sorption rate in each layer for the layered assemblies: (a) COMP; (b) COTN.

H_{cn} combined heat transfer coefficient at the clothing surface ($n = 0$, inner surface; $n = 1$, outer surface), W m^{-2} K^{-1}

h_{lg} mass transfer coefficient for evaporation and condensation, m s^{-1}

h_{mn} convective vapor transfer coefficient at the clothing surface ($n = 0$, inner surface; $n = 1$, outer surface), m s^{-1}

H_{mn} combined vapor transfer coefficient at the clothing surface ($n = 0$, inner surface; $n = 1$, outer surface), m s^{-1}

K_{fab} thermal conductivity of the fabric, W m^{-1} K^{-1}

I_{in} gap thickness with the neighbored layer for layer i ($n = 0$, left side; $n = 1$, right side)

K_l thermal conductivity of the liquid water, W m^{-1} K^{-1}

K_a thermal conductivity of the water vapor, W m^{-1} K^{-1}

K_{mix} effective Thermal conductivity of the fabric, W m^{-1} K^{-1}

L_i liquid conduct ratio of each layer

p-bar linearly averaged property of the fibers in layer i

P_{ti} general physical property of fiber type *ti*

r fiber radius, m

S_v surface volume ratio of the fiber, m^{-1}

T temperature of the fabric, K

T_{env} temperature of environment, K

tn total fiber type number a layer of fabric

W_{cf} water content of the fibers in the fabric, $W_{cf} = C_r/\rho$

β, *lc beta*	γ, *lc gamma*	Γ, *cap gamma*	ε, *lc curly epsilon*	
η, *lc eta*	θ, *lc theta*	λ, *lc lambda*	ξ, *lc xi*	κ, *lc kappa*
ρ, *lc rho*	σ, *lc sigma*	τ, *lc tau*	ϕ, *lc phi*	

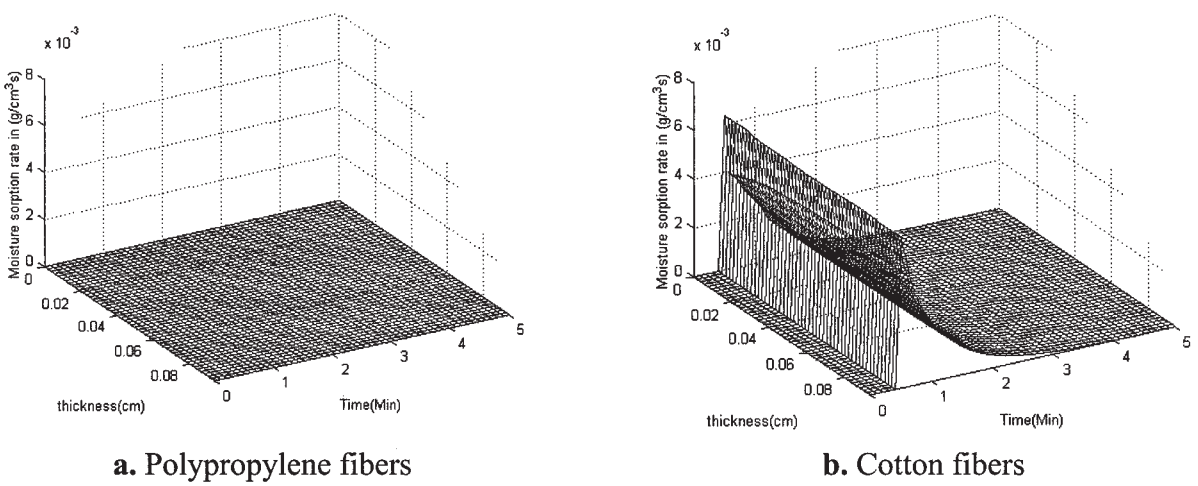

Figure 18 Dynamic fiber moisture sorption rate in the first layer of the COMP assemblies: (a) polypropylene fibers; (b) cotton fibers.

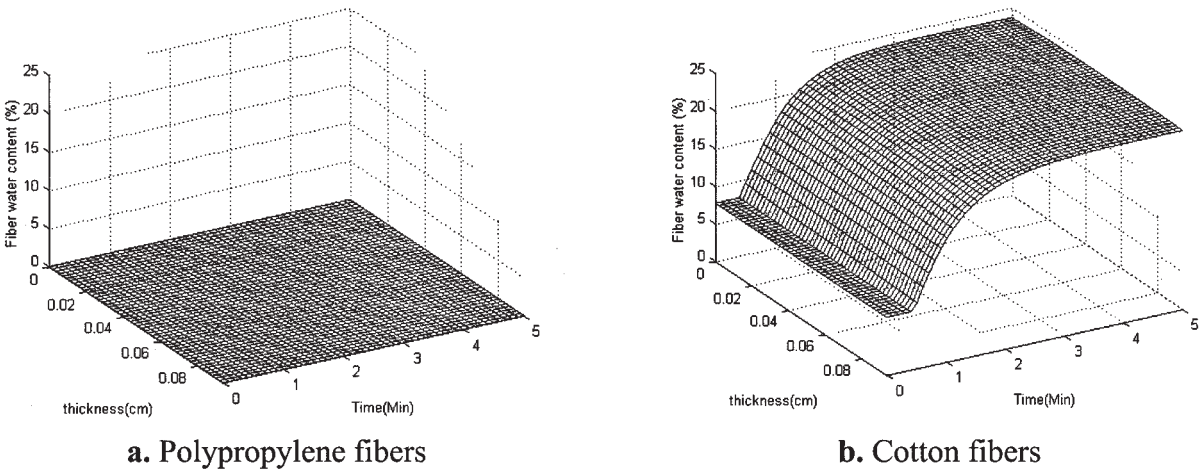

Figure 19 Dynamic fiber water content in the first layer of the COMP assemblies: (a) polypropylene fibers; (b) cotton fibers.

Greek letters

- β radiation absorption constant of the fiber, m^{-1}
- γ surface tension
- Γ_f effective sorption rate of the moisture, kg m^{-3} s^{-1}
- Γ_{lg} evaporation/condensation rate of the liquid/vapor, kg m^{-3} s^{-1}
- ε porosity of the fabric
- ε_a volume fraction of water vapor
- ε_f volume fraction of fibers
- ε_l volume fraction of liquid water
- ε_n emissivity of the clothing at the clothing surface ($n = 0$, inner surface; $n = 1$, outer surface)
- ε_r thermal emissivity of the fiber
- η dynamic viscosity of liquid, kg m^{-1} s^{-1}
- θ angle of incident of direct solar radiation
- κ_n proportions of mass transfer by vapor transport ($n = 1$) and by liquid water ($n = 2$)
- λ_{lg} heat of evaporation of water, kJ kg^{-1}
- λ_l heat of sorption or desorption of liquid water by fibers, kJ kg^{-1}
- λ_v heat of sorption or desorption of vapor by fibers, kJ kg^{-1}
- ξ_n proportions of moisture sorption at fiber surface covered by air ($n = 1$) and liquid water ($n = 2$)
- ρ density of the fibers, kg m^{-3}
- ρ_l density of the liquid water, kg m^{-3}
- σ Stefan–Boltzmann constant, 5.67×10^{-8} W m^{-2} K^{-1}
- τ_a effective tortuosity of the fabric for water vapor diffusion
- τ_l effective tortuosity of the fabric for liquid water diffusion
- ϕ contact angle of the liquid water on the fiber surface

References

1. Farnworth, B. Text Res J 1986, 56, 653.
2. Lotens, W. A.; Vandelinde, F. J. G.; Havenith, G. Ergonomics 1995, 38, 1114.
3. Lotens, W. A.; Pieters, A. M. J. Ergonomics 1995, 38, 1132.
4. Lotens, W. A.; Havenith, G. Ergonomics 1995, 38, 1092.
5. Gibson, P.; Charmchi, M. J Appl Polym Sci 1997, 64, 493.
6. Gibson, P. W.; Charmchi, M. Sen-1 Gakkaishi 1997, 53, 183.
7. Wang, Z.; Li, Y.; Zhu, Q. Y.; Luo, Z. X. J Appl Polym Sci 2003, 89, 2780.
8. Farnworth, B. Text Res J 1983, 53, 717.
9. Wang, Z.; et al. Sen-I Gakkaishi 2003, 59, 187.
10. Hu, J.-Y.; Li, Y.; Xu, W. L.; Wong, A. S. Text Res J 2004, 73.
11. Li, Y.; Zhu, Q. Y.; Luo, Z. X. Text Res J 2003, 73, 515.
12. Yao, M. Textile Material, 1st ed.; China Textile Press: Beijing, 1986.
13. Watt, I. C. Text Res J 1960, 30, 443.
14. Rae, A.; Bruce, R. In The Wira Textile Data Book; Wira, R., Ed.; State Mutual Book & Periodical Service: Leeds, UK, 1973.
15. Luo, Z. X.; Fan, J. T.; Li, Y. Int J Heat Mass Transfer 2000, 43, 2989.